AIP Journal of Applied Physics

Thermophysical properties and conduction mechanisms in AsxSe1−x chalcogenide glasses ranging from x = 0.2 to 0.5

Jason Lonergan, Charmayne Smith, Devon McClane, and Kathleen Richardson

Citation: Journal of Applied Physics **120**, 145101 (2016); doi: 10.1063/1.4962446
View online: http://dx.doi.org/10.1063/1.4962446
View Table of Contents: http://scitation.aip.org/content/aip/journal/jap/120/14?ver=pdfcov
Published by the AIP Publishing

Thermophysical properties and conduction mechanisms in As_xSe_{1-x} chalcogenide glasses ranging from x = 0.2 to 0.5

Jason Lonergan, Charmayne Smith, Devon McClane, and Kathleen Richardson
CREOL, The College of Optics and Photonics, University of Central Florida, Orlando, Florida 32816, USA

(Received 24 April 2016; accepted 28 August 2016; published online 11 October 2016)

The arsenic (As) to selenium (Se) ratio in As_xSe_{1-x} glasses ranging from x = 0.2 to 0.5 was varied in order to examine the effect of chemical and topological ordering on the glass' thermal transport behavior. The fundamental thermal properties of glass transition temperature (T_g), thermal conductivity (k), and heat capacity (c_p) were experimentally measured using differential scanning calorimetry, transient plane source method, and ultrasonic testing. Based on topological constraint theory, inflections in T_g and k were found at the structural coordination number $\langle r \rangle$ of 2.4, whereas a slight increase in heat capacity (c_p) with increasing $\langle r \rangle$ was observed. A maximum in total thermal conductivity of 0.232 W/m·K was measured for the composition with x = 0.4, which corresponds to the stoichiometric As_2Se_3. Gas kinetic theory was used to derive an expression for the photon (k_p) portion of thermal conductivity, which was calculated by measurements of the glass' absorption coefficient (α) and refractive index (n). Models based on Debye theory were used to derive expressions for specific heat (c_v) and the lattice (k_l) portion of thermal conductivity. The maximum value for k_p was 0.173 W/m·K for the composition with x = 0.2, and a minimum value of 0.144 W/m·K was measured for the composition with x = 0.4. Photonic conduction was found to be the dominant carrier mechanisms in all compositions, comprising 60% to 95% of the measured total thermal conductivity. *Published by AIP Publishing.* [http://dx.doi.org/10.1063/1.4962446]

I. INTRODUCTION

Chalcogenide glasses (ChGs) contain a chalcogen element, such as sulfur (S), selenium (Se), or tellurium (Te), and are usually accompanied by glass modifiers such as Arsenic (As), Antimony (Sb), Germanium (Ge), or Gallium (Ga).[1] ChGs generally exhibit high refractive indices, optical nonlinearity, photo-sensitivity, and phase-change ability.[2,3] Additionally, they have been evaluated using laser structural modification, making them attractive for diverse optical applications in bulk, thin film, and fiber form.[4–8] These properties make them suitable for systems including thermal imaging, night vision, CO and CO_2 laser power delivery, and remote chemical analysis.[9–14]

Rare earth (RE) doped chalcogenide (ChG) glasses have gained scientific interest due to their potential as optical amplifiers and laser gain media in the infrared (IR) waveband.[15] High quantum efficiency fluorescence in the IR regime is possible due to the low phonon energies (400–450 cm^{-1} in sulfides and 350 cm^{-1} in selenides),[16,17] which results in low non-radiative decay rates of rare earth energy levels. The low phonon energy is partially due to the large mass of the constituent atoms and the relatively weak bonds of the resulting structure.[17] Emission efficiency is further improved in ChGs by their high refractive index, which leads to high emission cross-sections.[15,18–21] Understanding fundamental heat transfer in well studied compositions such as binary As-Se glasses could lead to further insight into the interactions between photons and phonons, leading to further improvements in active optical properties.

Despite the attractive properties which have led to such expanded interest in the past decade, the full potential of multi-component ChGs has yet to be realized. This may be in part due to the demanding technical challenges of their synthesis and intrinsic limitations of their thermal and mechanical properties, defined by their chemical and structural make-up. Glasses must be quenched rapidly from a melt to prevent the reorganization of the atoms to a more favorable crystalline structure.[22] If the kinetics of glass formation are examined, the critical cooling rate required to yield a glass can be defined as

$$\frac{dT}{dt} \approx \frac{(T_m - T_n)D_T}{L_c^2}, \tag{1}$$

where T_m is the temperature of the melt at time zero, T_n represents the nose of the time-temperature-transformation (TTT) curve for the glass forming melt, D_T is the thermal diffusivity of the melt, and L_C is the maximum obtainable thickness of the glass.[22] Extremely low thermal diffusivity, low thermal shock resistance, and high coefficients of thermal expansion (CTE) can make processing of large, bulk ChG parts challenging.[23–27] Such attributes also impact ChG optical design, and fabrication approaches defined by glass viscosity, relaxation behavior, and thermo-optic properties which can directly impact manufacturing methods.[28–30] Thermal diffusivity, D_T, is directly related to total thermal conductivity, k_T, through Equation (2)

$$k_T = D_T c_p \rho, \tag{2}$$

where D_T is the thermal diffusivity, c_p is the heat capacity, and ρ is the bulk density.[31] Low thermal conductivity leads

to large, thermally induced stress gradients which can often lead to brittle fracture and catastrophic failure during the melt quench procedure caused by the relatively weak interatomic bonding present in most ChGs.[32] Understanding fundamental heat transfer in well studied binary ChG compositions such as As-Se will help enhance thermophysical properties and synthesis potential in more complex compositions.

There exists a large discrepancy in the reported thermal property values for binary As_xSe_{1-x} ChGs.[23,25–27] Examining one of the most widely studied compositions, stoichiometric As_2Se_3 has reported glass transition temperatures ranging from 167 to 196 °C which represents a 15% difference in T_g. Similar trends are observed in reported values for thermal conductivity, as values for stoichiometric As_2Se_3 range from 0.21 to 0.49 W/m·K which represents a factor of two variation. One source of discrepancies could be due to variations in glass processing routes leading to differences in thermal history and ultimately glass structure. The exact variations are hard to identify as some studies are vague or give little information on the melt quench method utilized.[25,33] Another source of discrepancy could also be due to differences of purity levels in the melted material, which are often not specified. Older studies (i.e., 1970s[25]) show data on glasses with purity levels around 3 N with no mention of annealing protocols used following glass formation, whereas more recent works cite 5 N purity elements in addition to utilizing post quench annealing procedures to reduce residual stresses.[1] With regards to conductivity measurements, there are multiple steady state and transient temperature measurement methods used within the literature.[23,25–27] Most steady state methods are performed by a comparative method in which a specimen is sandwiched between two reference materials in an insulated furnace, and thermal conductivity is determined through Fourier heat transfer analysis after the system has reached equilibrium. This method can be challenging due to multiple measurement points and the necessity of having the entire furnace at equilibrium. Transient methods involve a heat source or pulse in which the time-dependent temperature response of the material is then measured. This method is simpler than the steady state method, since no reference materials are needed and as little as one measurement point is required. Due to these differences in measurement methods, as well as material purity and processing conditions, reported values may not reflect the intrinsic thermal properties for high purity As-Se compositions.

This study aims to measure the fundamental thermophysical properties and determine the intrinsic heat transport mechanisms in high purity As_xSe_{1-x} compositions with x ranging from 0.2 to 0.5. A modern transient measurement technique will be used to systematically measure the overall thermal conductivity, k_T, around the floppy to rigid topological transition ($\langle r \rangle = 2.4$); this effort will separate k_T into its discrete photon, phonon (lattice), and electronic contributions to assess the dominant carrier mechanisms. Findings will be used to further understand how knowledge of these specific mechanisms can be employed in future design efforts to process ChG materials with targeted thermal properties.

II. THEORY

The fundamental metric used to describe the covalent network topology is the average coordination number, here denoted as $\langle r \rangle$.[34] For covalent glasses like chalcogenides, this number is computed based on the atomic (molar) fraction (f_i) of a given atomic component and that element's coordination number (m_i)

$$\langle r \rangle = \sum_i f_i m_i. \tag{3}$$

In this work, the coordination number is obtained by the "8-N" rule, where N is the number of valence electrons.[35–37]

Total thermal conductivity, k_T, is the measurement of a materials ability to transport thermal energy. Based on kinetic gas theory, this property can be expressed through Equation (4)

$$k_T = \sum_{i=l,e,p} \frac{1}{3} c_{p_i} v_i \lambda_i \rho, \tag{4}$$

where c_{p_i} is the heat capacity, v_i is the carrier velocity, λ_i is the mean free path of the carrier, and ρ is the bulk density.[38,39] Thermal energy can be transported through a solid material by three independent carrier mechanisms. These mechanisms include phonon transport (via the glass lattice's atomic bonds), electron transport (through free electron carriers), and photon transport (via material response to electromagnetic radiation).[38–40] Hence, total thermal conductivity, k_T, is comprised of a summation of lattice (k_l), photon (k_p), and electron (k_e) components as depicted in the following equation:

$$k_T = k_p + k_l + k_e. \tag{5}$$

In order to determine the relative photon, lattice, and electron fractions to the total thermal conductivity, k_T, several simplifying assumptions and continuum models were used. First, As-Se is an amorphous semiconductor with an electrical resistivity of $\sim 10^{12}$ Ω·cm at 300 K.[41] Using the Wiedemann–Franz law with the theoretical Lorenz number, the electronic portion of thermal conductivity, k_e, for As_2Se_3 would be expected to be small, calculated to be near 10^{-20} W/m·K. Based on this analysis, the electronic contribution has been ignored in the present work, leaving just photon and lattice thermal conductivity to be quantified. Although it is difficult to measure lattice thermal conductivity directly, a simple equation for photon conduction, k_p, can be derived from gas kinetic theory as[42,43]

$$k_p = \left(\frac{16}{3}\right) \frac{\sigma_{SB} n^2 T^3}{\alpha}, \tag{6}$$

where σ_{SB} is the Stephan–Boltzmann constant, n is the refractive index, T is the temperature, and α is the absorption coefficient for the material. Using Equation (6), photon thermal conduction can be calculated with measurements of the average absorption coefficient and refractive index over the transmissive regime. If k_e is ignored, and there is a direct measurement of k_T along with a calculation of k_p, k_l can be determined mathematically.

Debye's model of the phonon spectrum and Slack's model for high temperature ($T \gg \theta_D$) thermal conductivity

were used to verify the mathematical calculations of k_l. Both models are based on quantum mechanics principles of discrete vibrational energy levels. The Debye theory is based around the simplification that a linear relation exists for all angular phonon frequencies, $\omega(q,s))$, in the long-wavelength limit or for small wave numbers (q). s is an index which refers to phonon modes (i.e., longitudinal and transverse branches). Debye assumed a constant value $C(q,s) = C_D$ such that the maximum phonon frequency, or the Debye frequency, was equivalent to the following equation:[39]

$$\omega_d = C_d q_D = 2\pi v_D, \tag{7}$$

where v_D is the ordinary Debye frequency and q_D is the Debye wave number and can be expressed as

$$q_D = (6\pi^2 N/V)^{1/3} = (3\rho N_A r/4\pi\bar{M})^{1/3}, \tag{8}$$

where N is the number of atoms per unit volume, V is the crystal volume, r is the number of atoms in the molecule, $\bar{M}$ is the average molecular weight, N_A is Avagadro's number, and ρ is the density. In a real solid, C_D is anisotropic and different for longitudinal and transverse acoustic branches which can expressed by Equation (9)

$$\frac{3}{C_D^3} = \frac{1}{C_L^3} + \frac{2}{C_T^3}. \tag{9}$$

The Debye temperature for an acoustic phonon, shown in Eq. (10), is a measure of the maximum phonon frequency

$$\theta_D = \frac{h\omega_D}{k_B}, \tag{10}$$

where h is the Planck's constant and k_B is the Boltzmann's constant.[44] Combining Equation (7) through (10), the Debye temperature can be expressed as shown[45]

$$\theta_D = \frac{h\omega_D}{k_B} = \frac{h}{k_B}\left(\frac{3\rho N_A r}{4\pi\bar{M}}\right)^{1/3}\left(\frac{(1/C_L^3)+(2/C_T^3)}{3}\right)^{-1/3}. \tag{11}$$

By associating phonon energy with the vibration modes, the speed of sound within a solid can be used to determine the total energy of the lattice vibrations using Einstein-Bose statistics as shown in the following equation:[39,46,47]

$$U = 3\int_0^{E_{max}} \frac{E}{e^{E/k_B T} - 1} dE. \tag{12}$$

The phonon energy, E, can be expressed as

$$E = h\nu_i = \frac{hC_D s}{2\delta}, \tag{13}$$

where δ is the edge length of the unit cell. Therefore, the specific heat can be obtained by taking the derivative of Eq. (12), which gives the following expression:[39,46,47]

$$c_v = 9Nk_B\left[\frac{T}{\theta_D}\right]^3 \int_0^{\theta_D/T} \frac{x^4 e^x}{(e^x - 1)^2} dx, \tag{14}$$

where T is the temperature of the material and x is expressed as

$$x = \frac{hC_D s}{2\delta k_B T}. \tag{15}$$

A comprehensive model for the lattice thermal conductivity of a solid requires the knowledge of the phonon spectrum, Grüneisen constant, as well as an understanding of the various types of phonon scattering rates and their temperature and frequency dependencies. Morelli and Slack[44] developed a simplified model for lattice thermal conductivity for molecules with multiple atoms per unit cell. This model is applicable for materials at temperatures near or past the Debye temperature in which the Umklapp scattering process is the dominant mechanism. For these molecules, Morelli and Slack gave the following expression:[44,48]

$$k_l = A\frac{\bar{M}\theta_D^3 \delta}{\gamma^2 T P^{2/3}}, \tag{16}$$

where P is the atoms per unit cell and A is a constant based on the Grüneisen parameter, γ, as shown in the following equation:[49,50]

$$A = \frac{2.43 \cdot 10^{-8}}{1 - 0.514/\gamma + 0.228/\gamma^2}. \tag{17}$$

Therefore, with experimental or computational measurements of C_L, C_T, ρ, P, and δ, the thermophysical properties that arise from lattice vibrations within a solid can be simulated.

III. PROCEDURE

Twenty-five grams of high purity elemental starting materials (As: Alfa Aesar 5 N, Se: Alfa Aesar 5 N) were batched in 10 mm diameter quartz ampules inside a nitrogen purged glove box. After batching, the ampules were evacuated under vacuum (10^{-3} mm Hg) and sealed with a gas oxygen torch. The ampules were then heated to 700 °C for 12 h utilizing a ramp rate of 2 °C/min. The melts were constantly rocked to ensure melt homogeneity. After at least 12 h at 700 °C, the temperature was lowered to 600 °C, at which point the ampules were removed from the furnace and forced air quenched. Finally, each glass was annealed at 40 °C below its T_g for 12 h to ensure stress relaxation of the bulk structure.

Characteristic structure analyses were performed with density and Raman spectroscopy measurements, while temperature analysis was performed using glass transition temperature measurements. The density of the bulk glass was measured by the Archimedes' method using room temperature water as the submersion medium. The glass transition temperatures of the As-Se glasses were determined by a Netzsch (DSC F1 Phoenix, Boston, MA) differential scanning calorimeter (DSC). Bulk glass samples were cut using a diamond edge saw blade and crushed to a powder using a mortar and pestle. Approximately 20 mg of glass powder was sealed in an Al pan and heated at a rate of 10 °C/min in

the DSC. The glass transition temperature was taken as the inflection point of the endotherm in the heat flow curve. Information on the glassy structure was obtained through Raman analysis. The Raman spectra were measured with a resolution of 1 cm^{-1} using an average of 15 scans and were obtained by a Bruker SENTERRA Raman Microscope. The excitation was provided by a $\lambda = 785$ nm laser with an output power of 1 mW.

The average absorption coefficient for each composition was measured with both Fourier Transform Infra-Red (FTIR) (Thermo Scientific Nicolet is5) and UltraViolet-Visible (UV-Vis) spectroscopy (Cary 500 UV-Vis-NIR Spectrophotometer) at room temperature. For both techniques, the 10 mm diameter bulk glass rods were cut into nominally 2.0 mm thick slices. The discs were then ground and polished to a 0.5 μm finish. Transmittance (Tr) was collected with both the FTIR and UV-Vis, after background spectra were subtracted in order to account for ambient H_2O and CO_2. The experimental data were expressed in terms of intensity through the following equation:

$$Tr = \frac{I_T}{I_0}, \tag{18}$$

where I_T is the intensity of the light after it passes through the sample and I_o is the light intensity before the sample. The transmission curves were converted to absorbance (A) using Eq. (19)

$$A = \log_{10}\left(\frac{1}{Tr}\right) \tag{19}$$

and the absorption coefficient, α, was then related to absorbance by the relation shown in the following equation:

$$\alpha = \frac{A}{l}, \tag{20}$$

where l is the thickness of the specimen. The refractive indices of the bulk glasses were measured at a wavelength of 4.5 μm using a Metricon model 2010 M prism coupling system, at room temperature. These values were assumed constant for all transmissive wavelengths based on the literature that shows refractive index exhibited changes of only ~1% from 1.547 to 10.591 μm.[51] Samples were held in contact with a single crystal Ge measurement prism. The refractive index was measured 10 times to obtain an average with relative error ±0.0003. Details of the Metricon system and how it has been applied to ChG[52] can be found in the literature.[28,51]

The overall thermal conductivity (k_T) and specific heat capacity (c_v) were measured using the transient plane source (TPS) method (ThermTest, TPS 3500, Fredericton Canada). Specimens were cut from bulk glass rods to a nominal thickness of 2.5 mm and polished to 0.5 μm finish similar to those for spectroscopic measurements. The TPS sensor acts as both a heat source and resistance thermometer. As electric power is supplied to the sensor, the increase in mean temperature $T(\tau)$ of the specimen can be directly related to the variation in the sensor resistance $R(T)$ using Equation (21)

$$R(T(\tau)) = R_0[1 + \alpha_T(T(\tau) - T_0)], \tag{21}$$

where R_0 is the initial resistance at T_0, the initial temperature, and α_T is the temperature coefficient of resistance (TCR). The mean temperature of the sensor is given by Equation (22)

$$T(\tau) = \frac{P_i}{\pi^{3/2} r_s \kappa_T} D(\tau), \tag{22}$$

where P_i is the input power, r_s is the radius of the sensor, and $D(\tau)$ is a shape function. From Equation (22), k_T can be solved for algebraically. The specific heat was determined indirectly with Equation (23)

$$c_v = \frac{k_T}{D_T}, \tag{23}$$

where D_T is the thermal diffusivity. This can be obtained through Equations (21) and (24) based on a plot of the recorded temperature versus $D(\tau)$, where t is the time

$$D(\tau) = \sqrt{\frac{tD_T}{r_s^2}}. \tag{24}$$

Step wise, pulsed heating (power = 10 mW and pulse length = 0.1 s) was used to generate the resistively measured temperature–response curves. A minimum of five tests were performed for each data point, and the standard deviation is noted by the error bars shown (if no error bars are seen then they are within the size of the data points). c_v was converted to c_p through division by the measured specimen's density.

Transverse, C_T, and longitudinal, C_L, vibrational velocities for the calculation of the Debye frequency and temperature were measured using a Panametrics model 500PR Pulser-Reciever with 5 MHz longitudinal and transverse wave transducers (Panametrics Model V110 & V156, respectively). Short ultrasonic pulse waves were transmitted into the material, and the resulting back wall echoes were used to measure the acoustic velocities. Specimens were prepared identically to those measured with the TPS method. All sonic properties were measured at room temperature and ambient pressure.

IV. RESULTS AND DISCUSSION

A. Structure

Raman analysis was performed on all As_xSe_{1-x} compositions in order to gain insight into the changing bond structure of the glasses. Figure 1 shows the Raman shift data for select compositions spanning $\langle r \rangle = 2.2$ to 2.5. The spectra show a singular region in which multiple peaks corresponding to different structures are overlapping. Previous studies have attributed the large peak (240–260 cm^{-1}) to Se chain or ring-like fragments.[53–56] The large peak at 210–240 cm^{-1} has been attributed to $AsSe_3$ pyramidal units.[53,54,56] Finally, As_4Se_4 and As_4Se_3 cage-like molecules can be seen as a small shoulder (260–300 cm^{-1}).[53,54,56] At low coordination numbers, $\langle r \rangle = 2.2$ ($As_{0.2}Se_{0.8}$), we see a large peak around ~255 cm^{-1} indicating a large presence of Se chain fragments. A small peak is observed at 220 cm^{-1}, indicating the

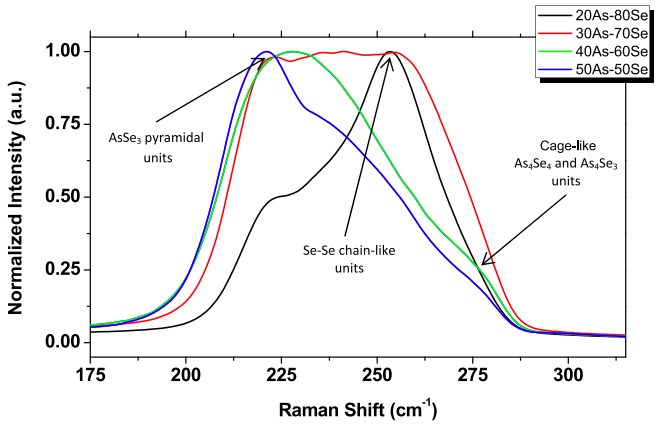

FIG. 1. Raman spectra of bulk As_xSe_{1-x} samples from x = 0.2 to 0.5.

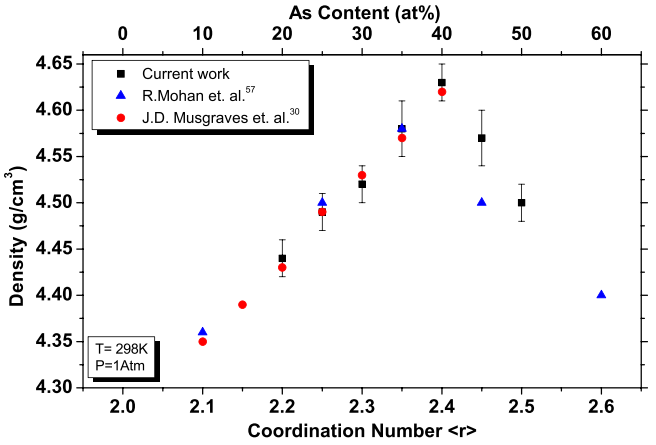

FIG. 2. Density of As-Se compositions with respect to the coordination number, ⟨r⟩. Values from this study and other references for the same series of As-Se materials are shown for comparison.

presence of $AsSe_3$ pyramidal units as well. The larger intensity of the peak at 255 cm^{-1} corresponds well to the floppy, chain-like structure predicted by topological constraint theory in this compositional space. As we increase the coordination number, $\langle r \rangle = 2.3$ ($As_{0.3}Se_{0.7}$), we see an increase in the peak intensity at 220 cm^{-1}, indicating that the structure is becoming more rigid and homopolar Se-Se bonds are being replaced by heteropolar As-Se bonds. At the topological transition coordination number of $\langle r \rangle = 2.4$ ($As_{0.4}Se_{0.6}$), the intensity of the 220 cm^{-1} compared to the 225 cm^{-1} peak is large. This indicates that the structure is predominantly As-Se bonding in the form of $AsSe_3$ pyramidal units. It should also be noted that the presence of a small shoulder at ~275 cm^{-1} emerges and indicates the formation of As_4Se_4 and As_4Se_3 cage-like structures. These cage-like structures correspond to the increased crosslinking and rigidity expressed in topological constraint theory around the transition number of $\langle r \rangle = 2.4$. Therefore, it has been experimentally verified that topological constraint theory is a suitable model in which to correlate structure changes in As_xSe_{1-x} glasses.

B. Physical and optical property characterization

To obtain the requisite inputs for the thermal property calculations defined above, various physical and optical property measurements were carried out on the target glass compositions including density, absorption coefficient, and refractive index.

The measured values for density, shown in Figure 2, agree well with the literature data for all compositions below $\langle r \rangle = 2.4$.[30,57] It should be noted that all data presented here are for studies which were performed on glasses made with As and Se of 5 N purity and density measurements which used the Archimedes' method with distilled water. The discrepancies in density above $\langle r \rangle = 2.5$ are most likely due to glass processing conditions, as the study by Mohan did not indicate melt, quench, or annealing temperature. Different structural units, such as the As_4Se_4 and As_4Se_3 units found in Se deficient glasses, could be more sensitive to kinetic conditions than longer Se chains found within Se rich glasses and cause the shift in trends seen above $\langle r \rangle = 2.4$. Therefore, changes in the kinetics due to quench temperature could result in differences in the final structure of the glass.

As can be seen in Figure 2, the density of the bulk glass increased linearly with increasing coordination number, ⟨r⟩, until $\langle r \rangle = 2.4$ and then decreased. The lowest measured density was 4.44 g/cm^3 for $As_{0.2}Se_{0.8}$ ($\langle r \rangle = 2.2$), and the highest density measured was 4.63 g/cm^3 for $As_{0.4}Se_{0.6}$ ($\langle r \rangle = 2.4$). The trend in density is consistent with topological constraint theory and Raman analysis. Compositions with low ⟨r⟩ values, and high Se contents, such as $As_{0.2}Se_{0.8}$ ($\langle r \rangle = 2.2$), contain loosely packed Se chain-like structures. The peak in density at $\langle r \rangle = 2.4$ is most likely due to the highly efficient packing of atoms correlating with the formation of As_2Se_3 pyramidal units. High ⟨r⟩ valued compositions such as $As_{0.5}Se_{0.5}$($\langle r \rangle > 2.4$) are made up of highly cross linked As-Se units in the form of both $AsSe_3$ pyramidal units and $As_4Se_{3(4)}$ cage-like units.[58,59] The decrease in density after $\langle r \rangle = 2.4$ indicates that the cage like units are less dense than the $AsSe_3$ pyramidal units. Therefore, as more and more homopolar bonds of either As-As (cage like units) or Se-Se (chain like units) are added, less efficient packing is observed. The effect of density on total thermal conductivity can be seen in Equations (2) and (4). Therefore, solely based on density, a maximum in total thermal conductivity would be expected at $\langle r \rangle = 2.4$.

As noted above, a key to quantifying the photonic contribution, k_p, to the overall k_T is an assessment of optical transport behavior within the glass. Figures 3(a) and 3(b) show the absorption coefficient versus wavelength measured by (a) UV-Vis spectroscopy and (b) FTIR spectroscopy for the seven As-Se compositions. A shift in the band edge towards the IR can be seen at the low wavelength band edge as the coordination number increases from $\langle r \rangle = 2.2$ to 2.4 (x = 0.2 to 0.4). Subsequently, a UV shift is seen with increasing coordination number after $\langle r \rangle = 2.4$ (compositions x = 0.45 and 0.5). The overall absorption coefficient increases beyond 12 μm when examining α across the glasses' transmissive regime in the infrared from ~0.8 μm to 18 μm. An inflection in α_{avg}, Table I, is once again observed at $\langle r \rangle = 2.4$ (x = 0.4) which can be explained by the correlation between optical band gap, absorption coefficient, and bond energy as shown in the following equation:

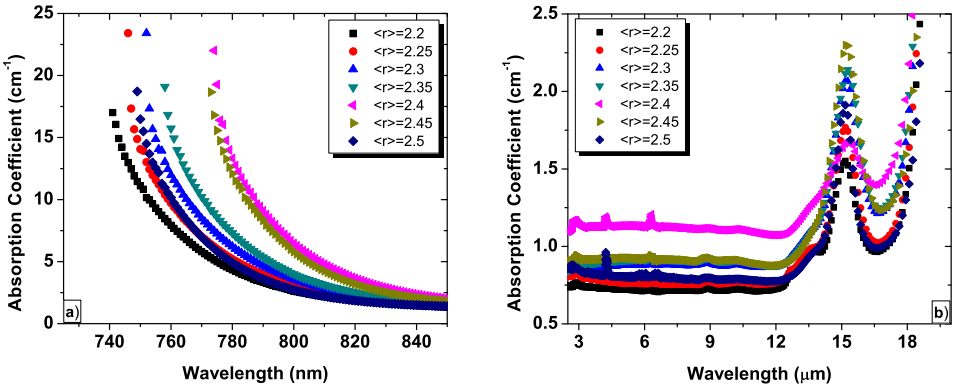

FIG. 3. Transmission spectra (in terms of absorption coefficient) measured from (a) UV-Vis spectroscopy and (b) FTIR spectroscopy on the glass compositions of interest (listed in terms of ⟨r⟩ values).

$$\alpha h\nu = B(h\nu - E_g)^r, \tag{25}$$

where E_g is the optical energy gap, B is a constant, and r is an index which can have a value of $^1/_2$ for allowed direct transition, 2 for allowed indirect transition, 3/2 for direct forbidden transition, and 3 for indirect forbidden transition.[31,56–59] For glasses such as those examined here, it would be expected to be 2. Assuming $h\nu$ is larger than E_g, this equation indicates that the absorption coefficient should increase as the optical band gap decreases and vice versa.

E_g was determined from a Tauc plot of $(\alpha h\nu)^{1/2}$ versus $h\nu$, and the resulting values can be found in Figure 4.[60] Trends with coordination number and composition are consistent with the reported literature on thin films, but the overall values are lower.[61] It has been shown that the optical band gap has a linear relationship with heat of formation as shown in the following equation:[62]

$$E_g = a(H_S - b). \tag{26}$$

Here, a and b are constants and H_S is the heat of formation. Literature values for bond energy (which is directly related to H_S) as well as measured physical and optical values can be seen in Table I.[32,63] Bond energy, and therefore H_S, will increase as ⟨r⟩ increases from 2.2 to 2.4 and decrease from 2.4 to 2.5. Hence, it is consistent that the observed trends in both band gap and absorption coefficient can be explained by the chemical ordering of the glass.

The relationship between the glass structure and absorption coefficient is also important to thermal properties as shown in Equation (6) which indicates that photonic thermal conduction should have an inverse relationship to the average optical absorption coefficient. Therefore, the portion of photonic conduction, k_p, to total thermal conductivity, k_T, would be expected to be dependent on absorption coefficient and decreases as ⟨r⟩ = 2.4 (x = 0.4) is approached.

Figure 5 shows a peak in refractive index at coordination number ⟨r⟩ = 2.4 (x = 0.4). The refractive index increases from ⟨r⟩ = 2.2 to 2.4 (x = 0.2 to 0.4) and decreases from ⟨r⟩ = 2.4 to 2.5 (compositions x = 0.45 and 0.5). The refractive index can be described by the single oscillator model proposed by Wemple and DiDomenico as shown in the following equation:[64,65]

$$n^2 = (E_d E_0)/(E_0^2 - E^2), \tag{27}$$

where n is the refractive index, E_0 is the average energy gap, E is the photon energy, and E_d is the dispersion energy. Assuming the E_d is the same for all specimens and given that E must be identical, since they were all tested at $\lambda = 4.5\ \mu$m, the refractive index can be expected to follow an inverse E_0 relationship. From Figure 4, it is known that E_0 has a minimum at ⟨r⟩ = 2.4; therefore, it is expected that a maximum refractive index would be seen at this point, which is observed. From Equation (6), the photonic thermal conductivity has a quadratic polynomial dependence with refractive index. Therefore, it is expected that the fractional portion of photonic conduction dependent on refractive index will increase as ⟨r⟩ = 2.4 is approached.

TABLE I. Coordination number, density, index, average absorption coefficient, and bond energy for As-Se compositions.

As *at.f.*	Se *at.f.*	⟨r⟩ C.N.	ρ (g/cm^3)	n a.u.	α_{avg} (cm^{-1})	Bond energy (kJ/mol)
0.5	0.5	2.5	4.5	2.6604	0.82	**As-As**
0.45	0.55	2.45	4.57	2.7432	0.92	183[63]
0.4	0.6	2.4	4.63	2.7916	1.13	**Se-Se**
0.35	0.65	2.35	4.58	2.7327	0.90	206[32]
0.3	0.7	2.3	4.52	2.6708	0.87	**As-Se**
0.25	0.75	2.25	4.49	2.6222	0.78	218[32]
0.2	0.8	2.2	4.44	2.5736	0.73	

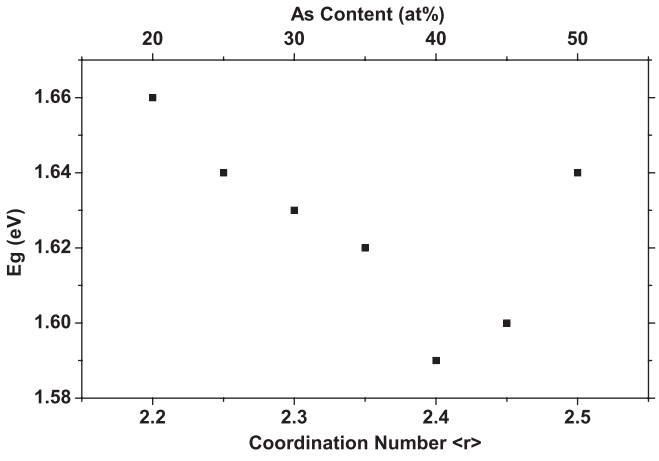

FIG. 4. Optical energy gap as determined from a Tauc plot of $(\alpha h\nu)^{1/2}$ versus $h\nu$.

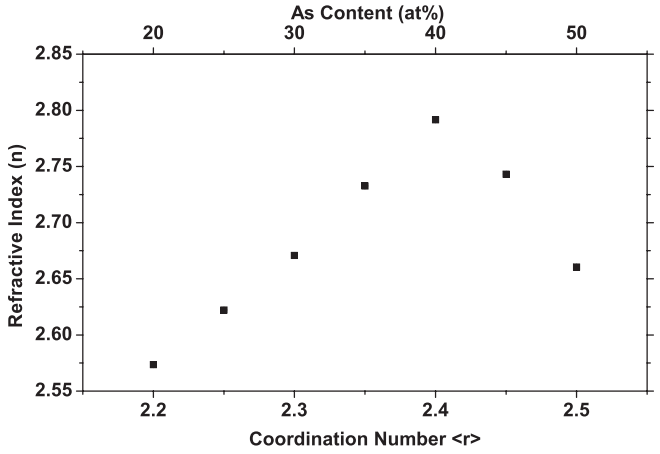

FIG. 5. Refractive index measurements performed at room temperature and $\lambda = 4.5\ \mu$m. Error bars reside within the data points and are generated from a minimum of ten measurements.

C. Thermal properties

Figure 6 shows the glass transition temperature (T_g) versus coordination number, $\langle r \rangle$, for the seven glass compositions in this study. Included are two commercially available stoichiometric As_2Se_3 glasses, along with glasses that were subjected to purification methods (Danto) to remove low levels of oxide impurity.[1,33,66–68] A summary of all thermal properties measured can be found in Table II. The lowest T_g for the current work was found to be 118 °C for $As_{0.2}Se_{0.8}$ ($\langle r \rangle = 2.2$), and the highest T_g was 203 °C for $As_{0.4}Se_{0.6}$ ($\langle r \rangle = 2.4$). Although the T_g values measured in this study are somewhat higher than previous measurements, it is worth noting the high purity starting powders and that Danto *et al.* observed an increase in T_g for increasing purity of As_2Se_3.[1] The trend in T_g with coordination number can be attributed to the mean atomic bonding energies of the glass structure. A glass with higher mean bonding energies will have a higher glass transition point as more energy is required to relax the structure and break bonds. As the As content increases, three-fold As atoms ($U_{As\text{-}Se} = 218$ kJ/mol) substitute for two-fold Se atoms ($U_{Se\text{-}Se} = 206$ kJ/mol) which

TABLE II. Glass transition temperature, heat capacity, total, photonic, and lattice thermal conductivity for As-Se compositions.

As *at.f.*	Se *at.f.*	$\langle r \rangle$ C.N.	T_g (°C)	c_p (J/g·K)	k_T (W/m·K)	k_p (W/m·K)	k_l (W/m·K)
0.5	0.5	2.5	184	0.298	0.166	0.159	0.007
0.45	0.55	2.45	200	0.260	0.199	0.154	0.045
0.4	0.6	2.4	203	0.288	0.232	0.144	0.088
0.35	0.65	2.35	167	0.240	0.217	0.161	0.056
0.3	0.7	2.3	147	0.258	0.210	0.170	0.040
0.25	0.75	2.25	129	0.278	0.196	0.171	0.025
0.2	0.8	2.2	118	0.261	0.188	0.173	0.015

increases the bonding energy, resulting in an increase in T_g.[32] A peak in T_g is measured at $\langle r \rangle = 2.4$ ($x = 0.4$) which corresponds to the unstressed rigid phase in which most of the bonding is heteropolar, As-Se, and the glassy structure is dominated by pyramidal $AsSe_3$ units. Further increase of the As content takes us into the stressed rigid phase in which the network is over constrained, and the presence of homopolar As-As ($U_{As\text{-}As} = 183$ kJ/mol) bonding and As_4Se_4 and As_4Se_3 cage-like molecule appear.[63] The lower energy of this bonding pair and these cage-like units contribute to a reduction in T_g. Therefore, the trends in T_g reflect the changing mean bond energy of the resulting compositions.

Figure 7 shows the heat capacity of the As-Se compositions with respect to the coordination number. Overall, a slight increase in heat capacity was observed from $\langle r \rangle = 2.2$ to 2.5 which corresponds to increasing As content. The lowest heat capacity was measured for $As_{0.35}Se_{0.65}$ ($\langle r \rangle = 2.35$) with 0.240 J/g·K, and the highest heat capacity was for $As_{0.5}Se_{0.5}$ ($\langle r \rangle = 2.5$) with 0.298 J/g·K. With the exception of the IRG 26 (SCHOTT) data, where the measurement technique was not defined, these values compare well with previously measured As-Se binary compositions.[49] Debye theory calculations were used in order to explain the overall trend from $\langle r \rangle = 2.2$ to 2.5. These values, along with calculated values for the Debye temperature, are found in Table III showing that θ_D varied from 135 to 167 K. It can be shown at high temperatures ($T \gg \theta_D$) that $x_D \ll 1$. If one assumes

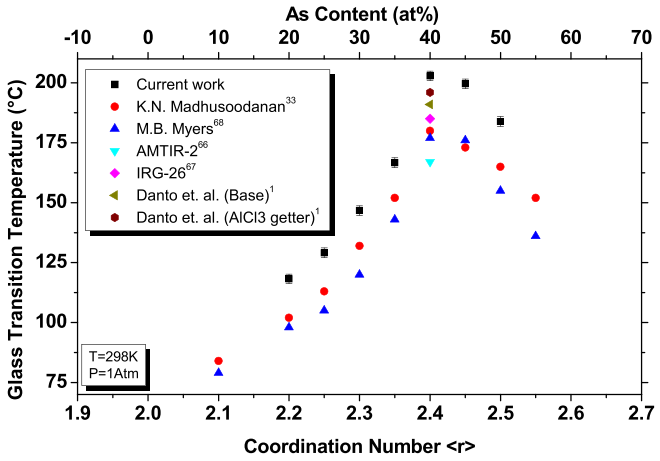

FIG. 6. Glass transition temperatures (T_g) of As-Se compositions as a function of coordination number. Other data for the same series of As-Se materials are shown for comparison.[1,33,66–68]

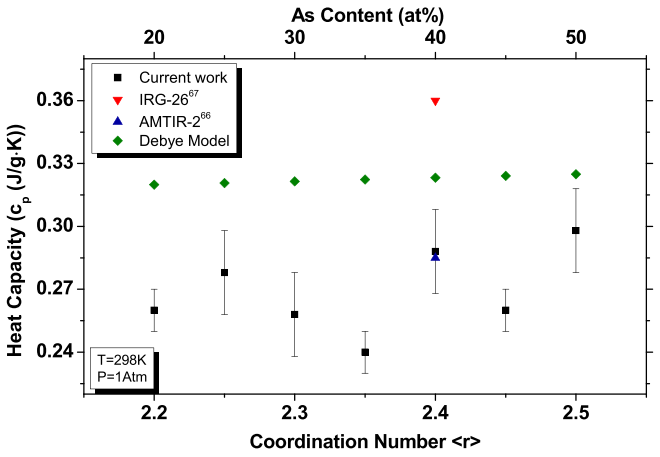

FIG. 7. Measured and calculated heat capacities versus coordination number for As-Se compositions at 25 °C.

TABLE III. Acoustic measurements and thermal property calculations using vibrational phonon theory.

As *at.f.*	Se *at.f.*	⟨r⟩ C.N.	C_L (m/s)	C_T (m/s)	ω_D (THz)	θ_D (K)	k_l Slack (W/m·K)	c_p Debye (J/g·K)
0.5	0.5	2.5	2062	1075	2.90	139	0.022	0.325
0.45	0.55	2.45	2230	1169	3.16	152	0.051	0.324
0.4	0.6	2.4	2353	1282	3.48	167	0.067	0.323
0.35	0.65	2.35	2247	1209	3.27	157	0.056	0.322
0.3	0.7	2.3	2211	1185	3.19	153	0.052	0.321
0.25	0.75	2.25	2074	1096	2.95	141	0.041	0.320
0.2	0.8	2.2	2052	1107	2.81	135	0.036	0.319

that room temperature qualifies as high temperature for As_xSe_{1-x} compositions, then Equation (14) reduces to

$$c_v \cong 3Nk\left(\frac{3}{x_D^3}\int_0^{x_D} x^2 dx\right) \approx 3Nk. \tag{28}$$

In the case of the high temperature limit, all specific heat values, c_v, should be invariant and approach a value of 25 J/mol·K, and the heat capacity, c_p, should have a trend which is inversely proportional to the molecular weight of each composition. This has been experimentally verified in other systems.[46,47] The calculated heat capacities, using the Debye model, for all As_xSe_{1-x} compositions are shown in Figure 7 and Table III. For the As_2Se_3 composition, this value would equate to a heat capacity of 0.323 J/g·K which is 11% higher than the measured value of 0.288 J/g·K. Therefore, the slight increase in heat capacity measured with increasing As content is consistent with measured acoustic velocities and Debye theory for the case of the high temperature limit.

Figure 8(a) shows total thermal conductivity values measured in this study at room temperature from ⟨r⟩ = 2.2 to 2.5 (x = 0.2 to 0.4) along with values reported from previous studies.[23,25–27] A large variation can be seen for these data across all coordination values; for example, the reported values for $As_{0.4}Se_{0.6}$ (⟨r⟩ = 2.4) vary from 0.21 W/m·K to 0.49 W/m·K.[23,25] This represents a variance of 57% amongst the reported values. The most likely reason for the large discrepancy as discussed earlier is the difference in testing methods. Both steady state and transient testing methods appear to follow similar trends. The steady state methods used by Alieva and Kuriyama yield values that are higher than the transient methods with a larger degree of scatter.[23,25] This scatter is most likely intrinsic to the steady state method based on the complexity of specimen fabrication and experimental setup. Contrary to the steady state method, all transient methods have values that lie close together and tend to agree on an overall trend. This is most likely due to the simplicity of sample fabrication as well as experimental setup which results in higher precision and accuracy. These data also agree with the published thermal conductivities for commercially available As_2Se_3 from Amorphous Materials and SCHOTT.[66,67] It is therefore likely that the transient testing methods are more accurate and represent more directly the intrinsic thermal properties of the As-Se compositions.

Figure 8(b) shows the total thermal conductivity values for measurements made only with transient measurement

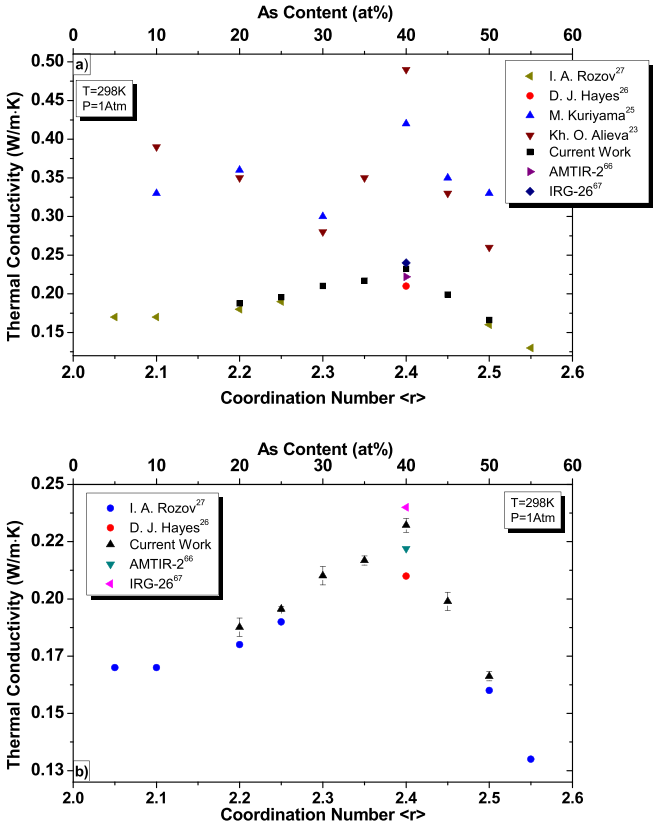

FIG. 8. Measured total thermal conductivity, k_T, values for (a) various measurement methods found in the literature and (b) k_T values obtained from transient technique measurements.

techniques. These data represent for the first time a transient method has been employed to systematically bridge the full coordination region from ⟨r⟩ = 2.2 to 2.5, as shown. The lowest thermal conductivity from the current study was 0.166 W/m·K measured for $As_{0.5}Se_{0.5}$ (⟨r⟩ = 2.5), and the highest total thermal conductivity was 0.232 W/m·K measured for $As_{0.4}Se_{0.6}$ (⟨r⟩ = 2.4). These reported values agree well with values reported from Rozov and Hayes, as well as data from commercial material datasheets showing an increase in total thermal conductivity from ⟨r⟩ = 2.2 to 2.4 and a decrease from ⟨r⟩ = 2.4 to 2.5.[26,27] Ultimately, the current study is the first study to systematically study thermal conductivity around the ⟨r⟩ = 2.4 topological and chemical ordering transition number, therefore systematically verifying that the highest thermal conductivities are indeed measured for As_2Se_3.

Figure 9 shows various contributions of photon thermal conductivity, k_p, and lattice (phonon) thermal conductivity, k_l, as calculated from the (measured) total thermal conductivity, k_T, using the equations and assumptions above. As can be seen, photonic thermal conductivity, k_p, decreases with increasing coordination number with an inflection at ⟨r⟩ = 2.4. The lowest measured photon conductivity is 0.144 W/m·K for $As_{0.4}Se_{0.6}$ (⟨r⟩ = 2.4), and the highest measured photon conductivity is 0.173 W/m·K for $As_{0.2}Se_{0.8}$ (⟨r⟩ = 2.2). This is opposite to the trend of lattice thermal conductivity in which a peak value of 0.088 W/m·K was determined at $As_{0.4}Se_{0.6}$ (⟨r⟩ = 2.4). One can interpret the decreasing photonic conduction around ⟨r⟩ = 2.4 based on the increasing absorption

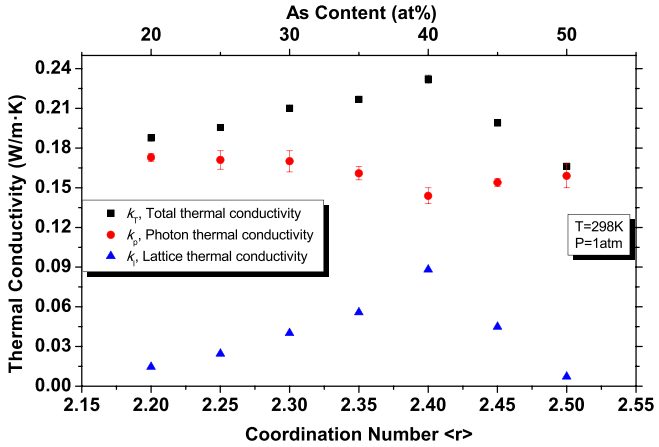

FIG. 9. Calculated thermal conductivity contributions (lattice and photon) for As-Se compositions as a function of coordination number.

coefficient of the glasses near this coordination number. Equation (6) shows that photon thermal conduction behaves inversely of the average absorption coefficient of the material. Therefore, as more radiation energy is absorbed and converted to lattice vibrations, less is available to optically transport thermal energy through the material. The increasing alpha of compositions as they approach $\langle r \rangle = 2.4$, as seen in Table I, clearly shows this is the case. Ultimately, the current measurements and calculations have shown that photonic conduction comprises anywhere from 60% to 95% of the total thermal conductivity of a binary As_x-Se_{1-x} glass at room temperature.

In order to further verify that photon conduction is the primary heat conduction mechanism, the total thermal conductivity, k_T, of $As_{0.4}Se_{0.6}$ was measured from $-150\,^{\circ}C$ to $150\,^{\circ}C$ which can be seen in Figure 10. From Equation (6), it would be expected that a material with photon dominated conduction would exhibit increasing total thermal conductivity with increasing temperature due to the T^3 dependence of photon conduction mechanism. With regards to the lattice conduction mechanism, Umklapp scattering should dominate and ultimately limit the lattice thermal conductivity above the Debye temperature, which is equivalent to $-106\,^{\circ}C$ for $As_{0.4}Se_{0.6}$ based on calculations made in this study. Therefore, the lattice heat conduction mechanism would decrease with either an exponential or inverse temperature dependence based on how far the temperature of the solid is from the Debye temperature of the material. Although the total thermal conductivity does not follow a T^3 trend, an increasing thermal conductivity for all temperatures is seen. Therefore, the measured behavior of total thermal conductivity with varying temperature agrees with the results found previously that As_xSe_{1-x} glasses are dominated by photon conduction mechanisms.

The trends in the lattice thermal conductivity were analyzed using the Slack model as shown in Equation (15). The model is ultimately meant for a crystalline lattice which required some assumptions to be made. The lattice parameter was chosen based on DFT glass structure simulations of As_2Se_3 in which the radial distribution function showed that the furthest spaced distribution of local connectivity was approximately 5.75 Å.[69] Similarly, the Grüneisen parameter was chosen to be $\gamma = 0.75$ based on crystalline chalcogen solids (ZnSe, CdTe to name a few) with low Debye temperatures ($\theta_D < 150\,K$).[48] Sound velocities and resulting Debye theory thermal property calculations can be found in Table III. The Slack model lattice thermal conductivities are plotted against the experimentally determined lattice thermal conductivities from previously in this study (Figure 11). It is immediately obvious that the Slack model does not predict the same degree of change with composition. For instance, the difference between the lowest measured lattice thermal conductivity ($As_{0.5}As_{0.5}$) and the highest ($As_{0.4}Se_{0.6}$) from the previously determined data is 92.1%, and the slack model predicts only a 47% change. Regardless of the ultimate accuracy of this phonon vibration based model, the predicted values are on the same order of magnitude and exhibit the same compositional trends as derived from the kinetic gas, photon transport based model. It should also be noted that the densities increased by 7% from $\langle r \rangle = 2.2$. to 2.4. This indicates that both topological and bond energy changes are responsible for the trends seen in lattice conductivity. Ultimately, the primary reason for the increase in lattice thermal conductivity as one approaches As_2Se_3 ($\langle r \rangle = 2.4$) is due to the increasing acoustic velocities. This correlates with an increase in bond energy which ultimately leads to increased phonon vibrational frequencies.[39]

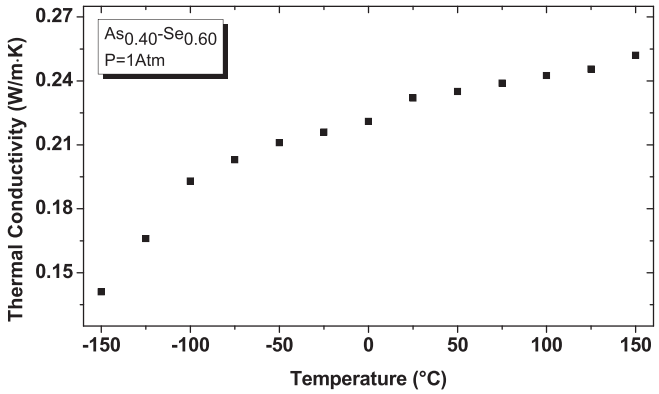

FIG. 10. Measured values of total thermal conductivity for $As_{0.4}Se_{0.6}$ from $-150\,^{\circ}C$ to $150\,^{\circ}C$.

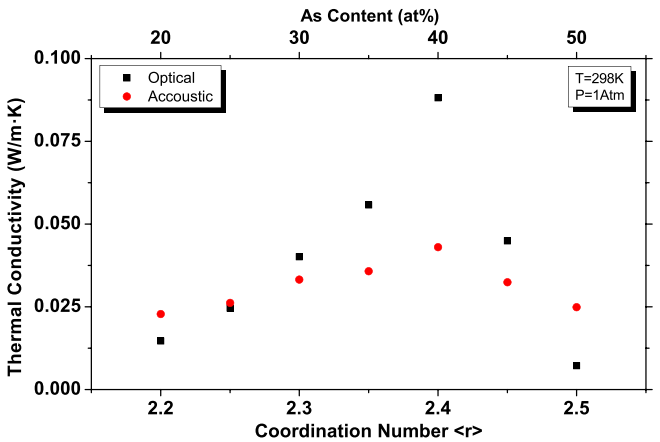

FIG. 11. Lattice thermal conductivity calculated using the Slack model compared to experimentally determined lattice thermal conductivity.

The reasons for the extremely low lattice thermal conductivity, below photon conduction even at room temperature, for As-Se glassy compositions are believed to be associated with several issues. The first reason for low lattice thermal conductivity in As-Se, and amorphous materials in general, is the lack of long range order. This leads to extremely low minimum free paths of the phonon carriers (λ). A value of 1.3 Å was determined by using Equation (4) to back calculate the mean phonon path length. This indicates that the average phonon wave within an As_xSe_{1-x} glass undergoes some form of scattering event, essentially after every atomic bond length. The second reason for the low lattice thermal conductivity for As-Se (compared, for instance, to a silicate glass) is the low bond energy, as these are directly related to bond stiffness and phonon carrier velocities.[39] For instance, the bond energy of As-Se is ~200 kJ/mol compared to that for a silicate glass in which the Si-O bond energy is ~450 kJ/mol, which results in a 2× reduction in bond energy in the ChG.[32,70]

From the calculations presented within this study, we have shown that the photonic conduction comprises anywhere from 60% to 95% of the total thermal conductivity of the binary As-Se glasses examined, greatly outweighing the lattice contribution. This lends quantitative evidence that thermal transport within As_xSe_{1-x} glasses, while impacted by, and directly proportional to, the glasses' lattice and extent of connectivity, is more dramatically impacted by the magnitude of intrinsic (optical) absorption. Despite the inflection at the topological $\langle r\rangle = 2.4$ value, the larger contribution of k_p clearly dominates thermal transport behavior. This then suggests that a highly coordinated ChG such as those largely employed in commercial applications will be limited in their conductivity by their optical transparency.

V. CONCLUSION

This study represents the first investigation aimed at quantifying the fractional thermal transport mechanisms seen in binary As_xSe_{1-x} compositions ranging from $x = 0.2$ to 0.5. High purity (5 N) elemental powders of both As and Se were melt quenched in the traditional manner, and these high purity glasses were examined using a transient measurement method (conductivity and heat capacity). Characteristic structure analysis (density) was performed on the same glasses to serve as inputs for calculations of specific heat capacity, and the highest density measured was 4.63 g/cm^3 for $As_{0.4}Se_{0.6}$ ($\langle r\rangle = 2.4$). In order to determine the photonic thermal conduction, the average absorption coefficient of the transmissive regime and the refractive index of the glasses were measured in the absorbing (UV-VIS) and transmissive (infrared) regions of the spectrum. The measured absorption coefficients, which ranged from 0.73 for $\langle r\rangle = 2.2$ to 1.13 for $\langle r\rangle = 2.4$, followed fundamental quantum mechanics based expressions based on bond energies which were then correlated with topological structure. Index data measured within the transmission window (4.5 μm) for the glasses obeyed the single oscillator model proposed by Wemple and DiDomenico. A peak in refractive index of $n = 2.7916$ was observed at coordination number $\langle r\rangle = 2.4$. The large discrepancy in the measured total thermal conductivity, k_T, compiled from this study and those of other efforts were found to be primarily due to measurement techniques (transient versus steady state) used. In addition, measured values of k_T for stoichiometric As_2Se_3 found in this study agree well with those published by commercial glass vendors.

Total thermal conductivity increased from $\langle r\rangle = 2.2$ to 2.4 with the highest total thermal conductivity measured for $As_{0.4}Se_{0.6}$ ($\langle r\rangle = 2.4$) with a value of 0.232 W/m·K. An inflection was observed at $\langle r\rangle = 2.4$ with the lowest thermal conductivity of 0.166 W/m·K measured for $As_{0.5}Se_{0.5}$ ($\langle r\rangle = 2.5$). The overall trend in total thermal conductivity k_T can be expressed by a derivation of the classical kinetic free gas model in which the changes in mean free path and carrier velocity can be used to explain property variation expected based on topological constraint and bond energy. The individual contributions to the overall thermal conductivity for both photon, k_p, and lattice thermal conductivity, k_l, were quantified for the first time. For stoichiometric As_2Se_3, a value of 0.144 W/m·K was measured for k_p and 0.088 W/m·K was measured for k_l. Photonic conduction was found to be the dominant carrier mechanisms in all compositions comprising anywhere from 60% to 95% of the total thermal conductivity.

ACKNOWLEDGMENTS

This research was supported in part with funding from the Defense Threat Reduction Agency (DTRA) under Contract No. HDTRA1-13-1-0001, and the U.S. Department of Energy Contract Nos. DE-EE0005327 and DE-NA000278.

[1]S. Danto, D. Thompson, P. Wachtel, J. D. Musgraves, and K. Richardson, "A comparative study of purification routes for As_2Se_3 chalcogenide glass," Int. J. Appl. Glass Sci. **4**(1), 31–41 (2013).
[2]A. B. Seddon, "Chalcogenide glasses: A review of their preparation, properties and applications," J. Non-Cryst. Solids **184**, 44–50 (1995).
[3]A. Zakery and S. R. Elliott, "Optical properties and applications of chalcogenide glasses: A review," J. Non-Cryst. Solids **330**, 1–12 (2003).
[4]B. J. Eggleton, B. Luther-Davies, and K. Richardson, "Chalcogenide photonics," Nat. Photonics **5**, 141–148 (2011).
[5]H. G. Dantanarayana, N. Abdel-Moneim, Z. Tang, L. Sojka, S. Sujecki, D. Furniss, A. B. Seddon, I. Kubat, O. Bang, and T. M. Benson, "Refractive index dispersion of chalcogenide glasses for ultra-high numerical-aperture fiber for mid-infrared supercontinuum generation," Opt. Mater. Express **4**(7), 1444–1455 (2014).
[6]J. D. Musgraves, K. Richardson, and H. Jain, "Laser-induced structural modification, its mechanisms, and applications in glassy optical materials," Opt. Mater. Express **1**(5), 921–935 (2011).
[7]L. Li, H. Lin, S. Qiao, Y. Zou, S. Danto, K. Richardson, J. D. Musgraves, N. Lu, and J. Hu, "Integrated flexible chalcogenide glass photonic devices," Nat. Photonics **8**, 643–649 (2014).
[8]Z. Tang, V. S. Shiryaev, D. Furniss, L. Sojka, S. Sujecki, T. M. Benson, A. B. Seddon, and M. F. Churbanov, "Low loss Ge-As-Se chalcogenide glass fiber, fabricated using extruded preform, for mid-infrared photonics," Opt. Mater. Express **5**(8), 1722–1737 (2015).
[9]A. F. Kosolapov, A. D. Pryamikov, A. S. Biriukov, V. S. Shiryaev, M. S. Astapovich, G. E. Snopatin, V. G. Plotnichenko, M. F. Churbanov, and E. M. Dianov, "Demonstration of CO_2-laser power delivery through chalcogenide-glass fiber with negative-curvature hollow core," Opt. Express **19**(25), 25723–25728 (2011).
[10]C. Plesa, D. Turcanu, C. Todirica, and I. Nicola, "Investigations on infrared chalcogenide glasses used in night vision devices," Chalcogenide Lett. **12**(11), 633–638 (2015).

[11]D. H. Cha, H.-J. Kim, Y. Hwang, J. C. Jeong, and J.-H. Kim, "Fabrication of molded chalcogenide-glass lens for thermal imaging applications," Appl. Opt. **51**(23), 5649–5656 (2012).
[12]J. Heo, M. Rodrigues, S. J. Saggese, and G. H. Sigel, Jr., "Remote fiber-optic chemical sensing using evanescent-wave interactions in chalcogenide glass fibers," Appl. Opt. **30**(27), 3944–3951 (1991).
[13]S. Sato, K. Igarashi, M. Taniwaki, K. Tanimoto, and Y. Kikuchi, "Multihundred-watt CO laser power delivery through chalcogenide glass fibers," Appl. Phys. Lett. **62**, 669–671 (1993).
[14]T. Arai and M. Kikuchi, "Carbon monoxide laser power delivery with an As2S3 infrared glass fiber," Appl. Opt. **23**(17), 3017–3019 (1984).
[15]R. Jing, Y. Guang, Z. Huidan, Z. Xianghua, Y. Yunxia, and C. Guorong, "Properties of Dy^{3+} doped Ge-As-Ga-Se chalcogenide glasses," J. Am. Ceram. Soc. **89**(8), 2486–2491 (2006).
[16]J. S. McCloy, B. J. Riley, D. A. Pierce, B. R. Johnson, and A. Qiao, "Infrared-transmitting glass-ceramics: A review," Proc. SPIE **8708**, Window and Dome Technologies and Materials XIII, 87080N (June 4, 2013) (2013).
[17]M. A. Hughes, "Modified chalcogenide glasses for optical device applications," in *Faculty of Engineering, Science and Mathematics Optoelectronics Research Centre*, Vol. Doctor of Philosophy (University of Southampton, Southampton, 2007).
[18]L. Sojka, Z. Tang, H. Zhu, E. Beres-Pawlik, D. Furniss, A. B. Seddon, T. M. Benson, and S. Sujecki, "Study of mid-infrared laser action in chalcogenide rare earth doped glass with Dy^{3+}, Pr^{3+} and Tb^{3+}," Opt. Mater. Express **2**(11), 1632 (2012).
[19]T. Schweizer, D. W. Hewak, D. N. Payne, T. Jensen, and G. Huber, "Rare-earth doped chalcogenide glass laser," Electron. Lett. **32**(7), 666–667 (1996).
[20]L. B. Shaw, B. Cole, P. A. Thielen, J. S. Sanghera, and I. D. Aggarwal, "Mid-wave IR and long-wave IR laser potential of rare-earth doped chalcogenide lass Fiber," IEEE J. Quantum Electron. **37**(9), 1127–1137 (2001).
[21]Y. Yan, R. Wang, K. Vu, S. Madden, K. Belay, R. Elliman, and B. Luther-Davies, "Photoluminescence in Er-doped Ge-As-Se chalcogenide thin films," Opt. Mater. Express **2**(9), 1270 (2012).
[22]J. E. Shelby, *Introduction to Glass Science and Technology* (Royal Society of Chemistry, Cambridge, UK, 2005).
[23]K. O. Alieva and S. A. Agaev, "The dependence of phonon thermal conduction of the chalcogenide glasses of the system As-Ge-Se on their composition (in Russian)," Fiz. Khim. Stekla **14**(5), 767–769 (1988).
[24]Kh. O. Amirkhanov, Ya. B. Magomedov, M. A. Aidamirov, Kh. O. Alieva, and S. M. Ismailov, "Thermal conductivity and electrical conductivity of chalcogenide glasses in the system $As_{30}Ge_{(x)}Se_{(70-x)}$ and their melts (in Russian)," Fiz. Khim. Stekla **58**(7–8), 302–303 (1982).
[25]M. Kuriyama, "Thermal conductivities of As-Se glasses," J. Am. Ceram. Soc. **58**(7–8), 302–303 (1975).
[26]D. J. Hayes, S. N. Rea, and A. R. Hilton, "Thermal conductivity of infrared transparent chalcogenide glasses," J. Am. Ceram. Soc. **58**(3–4), 135–137 (1975).
[27]I. A. Rozov, A. G. Chudnovskii, and V. F. Kokorina, "On the thermal conductivity of glassy semiconductors (in Russian)," Fiz. Tekh. Poluprovodn. **1**(8), 1159–1162 (1967).
[28]B. Gleason, "Designing optical properties in infrared glass," in *Materials Science and Engineering* (Clemson University, Clemson, 2016).
[29]E. Koontz, "Characterization of structural relaxation in inorganic glasses using length dilatometry," in *Materials Science and Engineering*, Vol. Doctor of Philosophy (Clemson University, Clemson, 2014).
[30]J. D. Musgraves, P. Wachtel, S. Novak, J. Wilkinson, and K. Richardson, "Composition dependence of the viscosity and other physical properties in the arsenic selenide glass system," J. Appl. Phys. **110**, 063503 (2011).
[31]W. D. Kingery and M. C. McQuarrie, "Thermal conductivity: I, concepts of measurement and factors affecting thermal conductivity of ceramic materials," J. Am. Ceram. Soc. **37**(2), 67–72 (1954).
[32]K. J. Rao and R. Mohan, "Chemical bond approach to determining conductivity band gaps in amorphous chalcogenides and pnictides," Solid State Commun. **39**(10), 1065–1068 (1981).
[33]K. N. Madhusoodanan and J. Philip, "Thermal transport near the glass transition in bulk As-Se glasses," Phys. Rev. B **39**(11), 7922–7927 (1989).
[34]A. K. Varshneya, A. N. Sreeram, and D. R. Swiler, "A review of the average coordination number concept in multicomponent chalcogenide glass systems," Phys. Chem. Glasses **34**(5), 179–193 (1993).
[35]J. Z. Liu and P. C. Taylor, "A general structural model for semiconducting glasses," Solid State Commun. **70**(1), 81–85 (1989).
[36]N. F. Mott, "Conduction in non-crystalline materials," Philos. Mag. **19**(160), 835–852 (1969).
[37]J. C. Phillips, "Topology of covalent non-crystalline solids I: Short-range order in chalcogenide alloys," J. Non-Cryst. Solids **34**(2), 153–181 (1979).
[38]T. M. Tritt, *Thermal Conductivity (Theory, Properties, and Applications)* (Kluwer Academic/Plenum Publishers, New York, 2004).
[39]G. Grimvall, *Thermophysical Properties of Materials* (Elsevier, Amsterdan, The Netherlands, 1999).
[40]J. R. Howell and R. Siegel, *Thermal Radiation Heat Transfer*, 3rd ed. (Hemisphere Publishing Corporation, Washington, DC, 1992).
[41]O. Madelung, U. Rossler, and M. Schulz, "Arsenic selenide (As_2Se_3) resistivity, mobility," in *Non-Tetrahedrally Bonded Elements and Binary Compounds I* (Springer, Berlin, Heidelberg, 1998), pp. 1–5.
[42]M. Zhao, X. Ren, and W. Pan, "Mechanical and thermal properties of simultaneously substituted pyrochlore compounds $(Ca_2Nb_2O_7)_x(Gd_2Zr_2O_7)1\text{-}x$," J. Eur. Ceram. Soc. **35**, 1055–1061 (2015).
[43]W. D. Kingery, H. K. Bowen, and D. R. Uhlmann, *Introduction to Ceramics* (John Wiley and Sons, Inc., New York, 1960).
[44]D. T. Morelli and G. A. Slack, "High lattice thermal conductivity solids," in *High Thermal Conductivity Materials*, edited by S. L. Shinde and J. S. Geola (Springer, New York, 2006).
[45]D. Bridge and A. A. Higazy, "Acoustic and optical Debye temperatures of the vitreous system $CoO\text{-}Co_2O_3\text{-}P_2O_5$," J. Mater. Sci. **21**, 2385–2390 (1986).
[46]C. Kittel, *Introduction to Solid State Physics*, 7th ed. (Wiley, 1996).
[47]D. V. Schroeder, *An Introduction to Thermal Physics* (Addison-Wesley, 2000).
[48]G. A. Slack, "The thermal conductivity of nonmetallic crystals," Solid State Phys. **34**, 1–71 (1979).
[49]G. Leibfried and E. Schlomann, Nachr. Akad. Wiss. Gottingen II **a(4)**, 71 (1954).
[50]C. L. Julian, Phys. Rev. **137**, A128 (1965).
[51]N. Carlie, N. C. Anheier, Jr., H. A. Qiao, B. Bernacki, M. C. Phillips, L. Petit, J. D. Musgraves, and K. Richardson, "Measurement of the refractive index dispersion of As_2Se_3 bulk glass and thin films prior to and after laser irradiation and annealing using prism coupling in the near- and mid-infrared spectral range," Rev. Sci. Instrum. **82**, 053103 (2011).
[52]B. Gleason, "Designing optical properties in infrared glass," in *Materials Science and Engineering* (Clemson University, Clemson, 2015).
[53]R. Golovchak, J. Oelgoetz, M. Vlcek, A. Esposito, A. Saiter, and J.-M. Saiter, "Complex structural rearrangements in As-Se glasses," J. Chem. Phys. **140**, 054505 (2014).
[54]M. S. Iovu, E. I. Kamitsos, C. P. E. Varsamis, P. Boolchand, and M. Popescu, "Raman spectra of $As_xSe_{100\text{-}x}$ and $As_{40}Se_{60}$ glasses doped with metals," Chalcogenide Lett. **2**(3), 21–25 (2005).
[55]V. N. Bogomolov, V. V. Poborchy, S. G. Romanov, and S. I. Shagin, "Raman spectra of chalcogen chains isolated in zeolite matrixes," J. Phys. C: Solid State Phys. **18**, L313–L317 (1985).
[56]R. Golovchak, A. Kovalskiy, A. C. Miller, H. Jain, and O. Shpotyuk, "Structure of Se-rich As-Se glasses by high-resolution x-ray photoelectron spectroscopy," Phys. Rev. B **76**, 125208 (2007).
[57]R. Mohan, T. S. Panchapagesan, and K. J. Rao, "Densities, microhardnesses, and electron microscopic studies of As-Se glasses," Bull. Mater. Sci. **3**(1), 29–36 (1981).
[58]P. S. Salmon, R. A. Martin, P. E. Mason, and G. J. Cuello, "Topological versus chemical ordering in network glasses at intermediate and extended length scales," Nature **435**, 75–78 (2005).
[59]P. Boolchand, X. Feng, and W. J. Bresser, "Rigidity transitions in binary Ge-Se glasses and the intermediate phase," J. Non-Cryst. Solids **293–295**, 348–356 (2001).
[60]J. Tauc, "Optical properties and electronic structure of amorphous Ge and Si," Mater. Res. Bull. **3**, 37–46 (1968).
[61]K. Tanaka, "Structural phase transitions in chalcogenide glasses," Phys. Rev. B **39**(2), 1270–1279 (1989).
[62]A. A. Otham, K. A. Aly, and A. M. Abousehly, "Effect of Te additions on the optical properties of (As-Sb-Se) thin films," Thin Solid Films **515**, 3507–3512 (2007).
[63]L. Tichy and H. Ticha, "Covalent bond approach to the glass-transition temperature of chalcogenide glasses," J. Non-Cryst. Solids **189**(1–2), 141–146 (1995).
[64]S. H. Wemple, "Refractive-index behavior of amorphous semiconductors and glasses," Phys. Rev. B **7**(8), 3767–3777 (1973).
[65]S. H. Wemple and M. DiDomenico, Jr., "Behavior of the electronic dielectric constant in cobalent and ionic materials," Phys. Rev. B **3**(4), 1338–1351 (1971).

[66]Amorphous Materials, AMTIR-2, 2013.
[67]S. G. Inc., Infrared Chalcogenide Glasses-IRG 26, 2013.
[68]M. B. Myers and E. J. Felty, "Structural characterizations of vitreous inorganic polymers by thermal studies," Mater. Res. Bull. **2**, 535–546 (1967).
[69]M. Bauchy and M. Micoulaut, "Structure of As2Se3 and As-Se network glasses: Evidence for coordination defects and homopolar bonding," J. Non-Cryst. Solids **377**, 34–38 (2013).
[70]A. K. Varshneya, *Fundamentals of Inorganic Glasses* (Academic Press, Inc., New York, 1994).